metals

MDPI

Article

Surface Enhancement of CoCrMo Bioimplant Alloy via Nanosecond and Femtosecond Laser Processing with Thermal Treatment

Hsuan-Kai Lin [1,*], Po-Wei Chang [1], Yu-Ming Ding [1], Yu-Ting Lyu [2], Yuan-Jen Chang [3] and Wei-Hua Lu [1,*]

[1] Department of Materials Engineering, National Pingtung University of Science and Technology, Pingtung 912, Taiwan; m11345005@mail.npust.edu.tw (P.-W.C.); m11345003@mail.npust.edu.tw (Y.-M.D.)
[2] Metal Industries Research and Development Centre (MIRDC), Kaohsiung City 811, Taiwan; lyting@mail.mirdc.org.tw
[3] Department of Mechanical Engineering, National Taipei University of Technology, Tapei 106344, Taiwan; yjchang@ntut.edu.tw
* Correspondence: hklin@mail.npust.edu.tw (H.-K.L.); whl@mail.npust.edu.tw (W.-H.L.); Tel.: +886-8-7703202-7568 (H.-K.L.); +886-8-7703202-7554 (W.-H.L.)

Abstract

With an aging population, the number of joint replacement surgeries is on the rise. One of the most common implant materials is cobalt–chromium–molybdenum (CoCrMo) alloy. Hence, the surface properties of this alloy have attracted increasing attention. In this study, nanosecond and femtosecond laser processing, followed by annealing, was employed to modify the CoCrMo surface. The effects of the treatment conditions on the surface morphology, structure, composition, hardness, roughness, contact angle, wear properties, and corrosion current were studied. Femtosecond laser processing with an energy density of 1273 mJ/cm^2, followed by heat treatment at 160 °C for 2 h, produced laser-induced periodic surface structures (LIPSS) without altering the chemical composition of the alloy and rendered the surface superhydrophobic. In contrast, nanosecond laser treatment at higher laser energy densities promoted the formation of an oxide layer, which improved the hardness and corrosion resistance of the substrate. Overall, the CoCrMo samples processed using the femtosecond laser system exhibited superior corrosion and wear resistance, with a protection efficiency of approximately 92%.

Keywords: CoCrMo; nanosecond and femtosecond lasers; annealing treatment; wear; corrosion resistance

Academic Editor: Gabriel A. Lopez

Received: 2 August 2025
Revised: 26 August 2025
Accepted: 28 August 2025
Published: 1 September 2025

Citation: Lin, H.-K.; Chang, P.-W.; Ding, Y.-M.; Lyu, Y.-T.; Chang, Y.-J.; Lu, W.-H. Surface Enhancement of CoCrMo Bioimplant Alloy via Nanosecond and Femtosecond Laser Processing with Thermal Treatment. *Metals* **2025**, *15*, 980. https://doi.org/10.3390/met15090980

1. Introduction

Advances in healthcare, nutrition, and living standards have resulted in an aging population in many regions worldwide. This, in turn, has led to a higher prevalence of degenerative arthritis and other joint-related disorders. According to the World Health Organization, the number of people affected by degenerative arthritis was predicted to rise globally between 2017 and 2024, with the elderly population accounting for a large proportion of those affected (approximately 50%) [1]. Traditional treatments, such as medication, can provide temporary relief; however, they fail to address the underlying causes. Accordingly, artificial joint replacement is often regarded as a more effective long-term solution.

High-quality artificial joints must satisfy five fundamental criteria: good biocompatibility, high corrosion resistance, superior mechanical properties, enhanced wear resistance, and effective osseointegration. Various materials are used for biomedical implants, including titanium alloy (Ti6Al4V) [2,3], stainless steel (SSL) [4], and cobalt chromium molybdenum (CoCrMo) alloys [5,6]. Among these materials, CoCrMo is one of the most commonly used owing to its excellent mechanical properties, corrosion resistance, and biocompatibility [7–9]. However, CoCrMo alloy joints are subjected to complex and varying loads during in vivo service, which can lead to unbalanced wear of the metal surface and potential joint failure [10]. Consequently, the surface properties of CoCrMo are of significant interest for ensuring the long-term success of the joint. Many surface modification treatments have been developed to enhance the wear resistance of alloys, such as doping [11], plasma surface treatment [12], chemical vapor deposition (CVD) [13], physical vapor deposition (PVD) [14], and laser processing [15,16]. However, many of these methods are constrained by factors such as implant geometry, size, and coating adhesion. For instance, plasma treatment suffers from limited controllability and poor repeatability, while PVD requires a high-vacuum environment and incurs a high processing cost. Laser processing offers several advantages over these techniques, including higher flexibility, localized treatment capability, faster processing speed, smaller heat-affected zone, and improved compatibility with automated systems. Numerous studies have demonstrated that laser surface modification can significantly enhance the surface properties and tribological performance of metallic alloys.

NgO and Chun [17] employed a nanosecond laser with a wavelength of 355 nm in combination with heat treatment at 100 °C to modify the surface of stainless steel. The resulting surface exhibited both superhydrophobicity and excellent self-cleaning properties. Compared to nanosecond lasers, femtosecond lasers offer several advantages, including nanoscale precision, negligible heat-affected zones (HAZ), smooth post-processed surfaces, and broad material compatibility [18]. Yang et al. [19] showed that the application of femtosecond laser treatment to titanium substrates generated periodic nanostructures that significantly increased the contact angle and enhanced the corrosion resistance.

However, the literature contains scant information about the combined effects of laser pulse width (ns vs. fs) and post-annealing on the surface properties of CoCrMo alloys. The present study addresses this gap by evaluating the effects of different laser systems on the surface morphology, wettability, wear behavior, and electrocorrosion resistance of CoCrMo alloy plates. Three laser systems were used: two nanosecond lasers with wavelengths of 1064 and 355 nm, and one femtosecond laser with a wavelength of 1030 nm. All laser-treated samples were annealed at 160 °C to investigate the synergistic effects of laser processing and thermal treatment. The resulting surface morphologies and wettability were characterized and correlated with the observed improvements in the corrosion resistance and wear performance of the samples.

2. Materials and Methods

CoCrMo alloy with a composition of 63 wt.% Co, 31 wt.% Cr, 4 wt.% Mo, and minor amounts of O and other elements (totaling 2 wt.%) were obtained from Gloria Material Technology Corp. (Tainan city, Taiwan). The material was sectioned into plates with a thickness of approximately 2 mm, and the surfaces were then ground sequentially using silicon carbide papers ranging from #200 to #2000 grit size. After grinding, the sample surfaces were polished with alumina powder (particle size of approximately 1 μm) to obtain a mirror-like finish. The polished samples were processed using three laser systems with different wavelengths and pulse widths: (1) UV (Coherent AVIA 355-7000, Coherent corp., Santa Clara, CA, USA), (2) IR (G3 SM Series 12 W Pulsed Fiber Laser, SPI, Southampton, Hampshire, UK), and femtosecond (Laser P 400 U, GF, Biel, Switzerland). The

laser processing parameters are presented in Table 1. The laser wavelengths and pulse durations were selected to represent typical ranges for nanosecond and femtosecond laser systems used in metallic surface modification studies. Moreover, the energy density levels were chosen to encompass the threshold regimes for observable surface texturing and oxidation [20]. For each laser treatment, the overlap percentage, pulse energy, and energy density were calculated as follows:

$$\text{Overlapping (\%)} = \left[1 - \left(\frac{\text{Speed}}{\text{D} \times \text{kHz}}\right)\right] \times 100\% \quad (1)$$

$$\text{Pulse energy (μJ)} = \left(\frac{\text{W}}{\text{kHz}}\right) \quad (2)$$

$$\text{Energy density } \left({}^{\text{mJ}}/_{\text{cm}^2}\right) = \left\{\frac{\text{Pulse energy}}{\pi\left[\left(\frac{\text{D}}{2}\right)^2\right]}\right\} \quad (3)$$

where D is the spot size (μm), W is the laser power (W), kHz is the pulse frequency (kHz), and speed is the scanning speed (mm/s).

The laser-treated samples were heated at 160 °C on a hot plate (JP-20D, Shin Kwang Machinery Industry Co., Ltd., Taipei City, Taiwan) for 2 h to stabilize the laser-induced structures and enhance surface properties. The surface morphologies of the samples were observed using a Field-Emission Scanning Electron Microscope (FE-SEM, JSM-7600F, JEOL Ltd, Tokyo, Japan) equipped with Energy-Dispersive X-ray Spectrometry (EDS, X-MAX50, Oxford Instruments, Oxford, UK). The crystal structures were examined by X-ray Diffraction (XRD, Bruker D8 Advance, Bruker Company, Billerica, MA, USA) using Cu-Kα radiation (λ = 0.154 nm) at operating voltages and currents of 40 kV and 40 mA. Grazing-incidence X-ray diffraction (GIXRD) measurements were carried out with a fixed incident angle of 0.7° to enhance surface sensitivity and minimize substrate contributions. The diffraction patterns were collected over a 2θ range of 20–80° with a step size of 0.04° and a counting time of 0.5 s per step. The surface hardness was measured using a Vickers hardness tester (Mitutoyo HM-113, Mitutoyo Corporation, Kawasaki, Japan) with an applied load of 10 kg. The surface roughness was determined using an Alpha-Step profiler (P6, KLA Corporation, Milpitas, CA, USA) at a speed of 20 μm/s, measurement distance of 200 μm, and applied load of 1 mg. Wettability was evaluated using deionized water droplets with a volume of 1 μL and a contact angle measuring system (OCA-15EC, DataPhysics Instruments GmbH, Filderstadt, Germany). The wear resistance of the samples was evaluated using a slow-speed cutting machine (Buehler, IsoMet, Lake Bluff, IL, USA) fitted with a stainless steel abrasive wheel with a diameter of 100 mm and a thickness of 5 mm. For all wear tests, the rotational speed of the wheel was set to 100 rpm, the normal contact load was 1075 g, and the wear time was 120 min. Water was used as the wet-abrasion medium for all samples. The electrochemical characteristics and corrosion behavior of the samples were evaluated in 0.9% NaCl solution using an electrochemical analyzer (CHI 6119E, CH Instruments, Bee Cave, TX, USA). Electrochemical tests were performed at 37 °C over a potential range of −1 to 1 V with a scanning rate of 1 mV/s.

Table 1. Parameter settings for different laser systems.

Wavelength	**1064 nm**	**355 nm**	**1030 nm**
Pulse width	26 ns	30 ns	258 fs
Scan speed		50 mm/s	
Frequency		50 kHz	
Spot size	35 μm	17 μm	30 μm
Overlapping	97.14%	94.11%	96.67%
Energy density	1039, 3118, 5197 mJ/cm²	1322, 2643, 3965 mJ/cm²	1273, 1556, 1839 mJ/cm²

3. Results

3.1. Subsection Microstructural Features and Elemental Distributions, and Crystal Structures of CoCrMo Samples Subjected to Laser Processing

Figure 1 shows the surface morphologies of the CoCrMo samples treated with different laser systems and energy densities. At low energy densities (1039–1322 mJ/cm^2), no laser-scanning traces were observed on the surfaces treated with nanosecond lasers. However, femtosecond laser treatment produced well-defined laser-induced periodic surface structures (LIPSS) on the treated surface. The LIPSS microstructures were aligned with the laser polarization direction and formed circular patterns with a characteristic period of approximately 1.05 µm. As the energy density increased, ablation marks and splatter-induced structures were observed on nanosecond-treated surfaces. Of the two wavelengths, the 355 nm laser produced a broader ablation area than the 1064 nm laser. For femtosecond lasers, a higher energy density causes the LIPSS structures to disappear owing to structural degradation or melting of the surface features [21]. Figure 2 shows the oxygen content of the laser-treated CoCrMo alloy surfaces as a function of energy density. For all laser systems, the surface oxidation effect significantly increased with increasing energy density. Among the three systems, the 355 nm nanosecond laser system generally resulted in the highest oxygen content, particularly at higher energy densities. However, at low energy densities, the oxygen content across all three systems was broadly comparable to that of the untreated surface (Figure 3). Fava et al. [22] demonstrated surface oxidation and compositional changes of CoCrMo alloys within the first few nanometers by an X-ray photoelectron spectroscopy (XPS) analysis. Our EDS results showed a similar trend, which is consistent with this reference and supports our conclusions regarding surface modification. Notably, the highest oxygen content (6%) was observed in the sample processed using a femtosecond laser. Figure 4 shows XRD patterns of the original CoCrMo sample and the three laser-processed samples. Energy densities of 1039, 1322, and 1273 mJ/cm^2 were applied for the different laser systems. The original sample exhibited a dual-phase structure consisting of hexagonal close-packed (HCP) and face-centered cubic (FCC) phases.

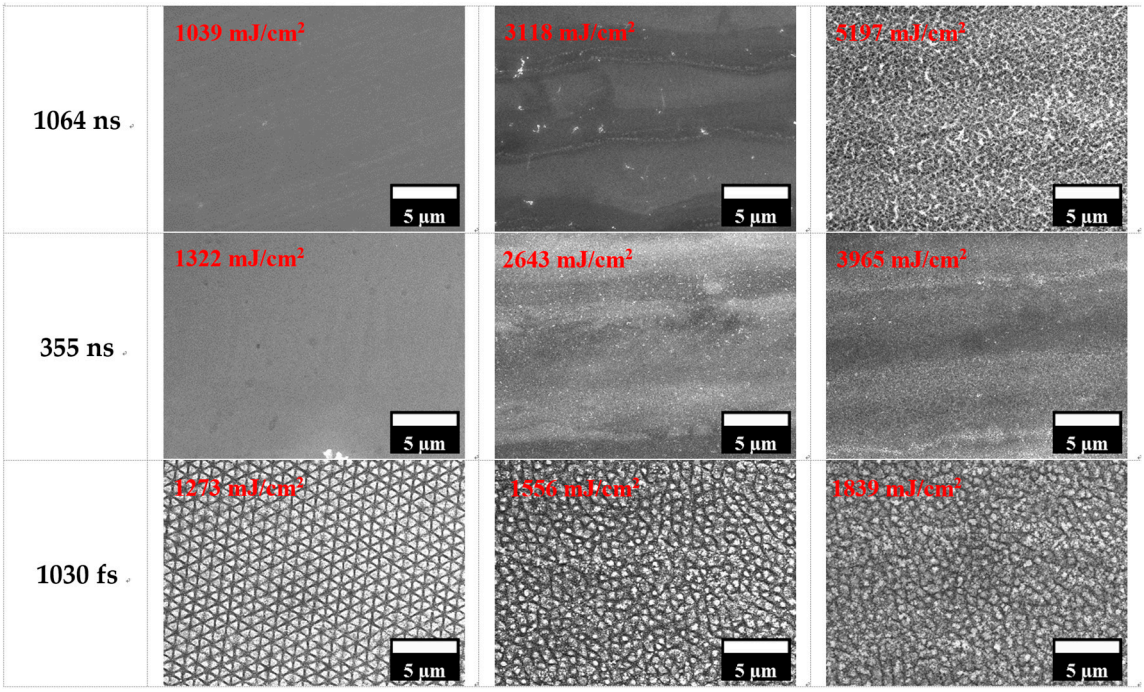

Figure 1. SEM images showing surface morphologies of CoCrMo samples following laser treatment with different pulse durations, wavelengths, and energy densities.

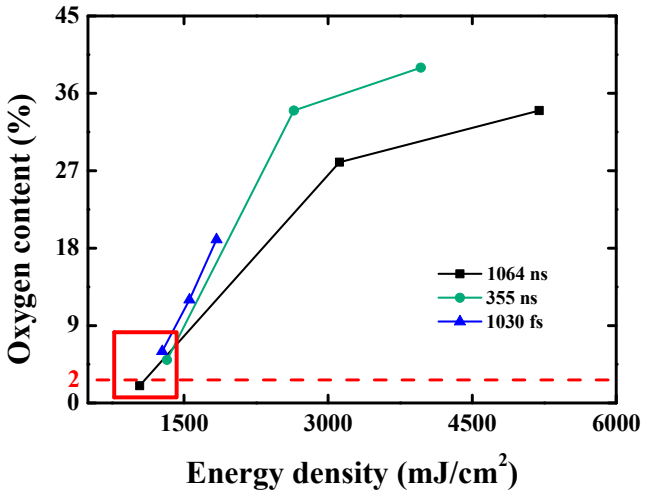

Figure 2. Surface oxygen content of CoCrMo samples after laser treatment and the dotted line represented the initial oxygen content of raw CoCrMo sample.

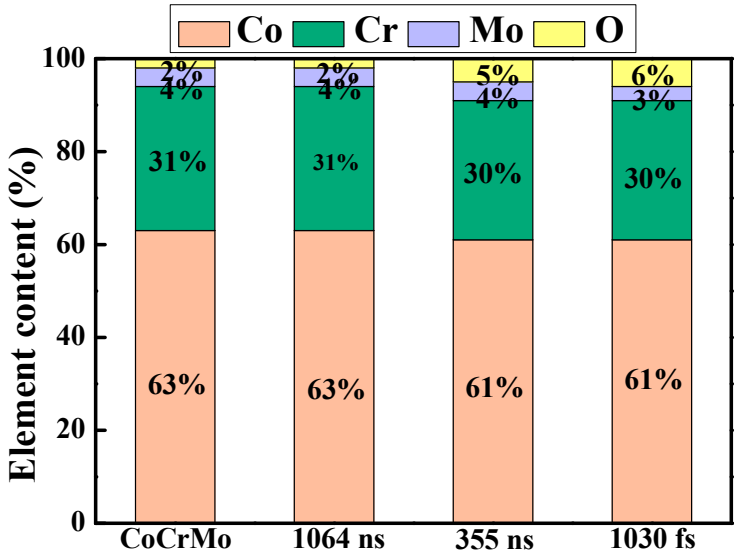

Figure 3. Elemental compositions of CoCrMo samples after low-energy-density laser treatment.

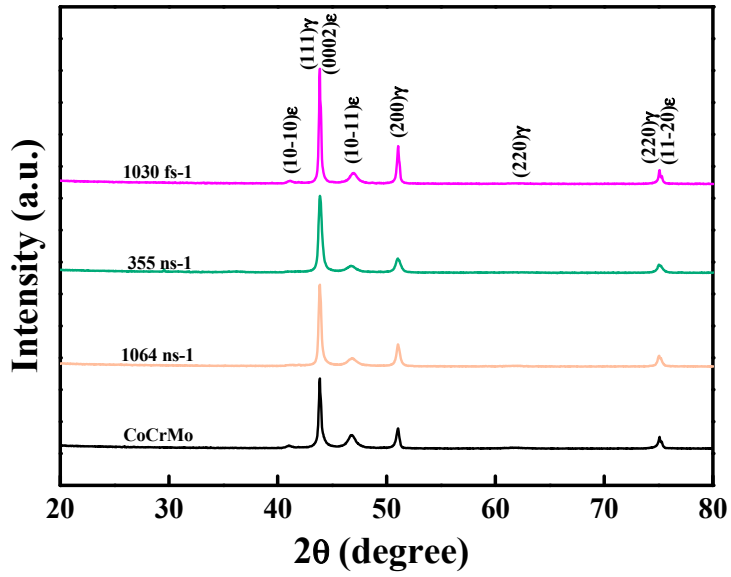

Figure 4. XRD patterns of CoCrMo samples after laser treatment.

3.2. Surface Roughness, Hardness, and Wettability of Laser-Treated CoCrMo Samples Processed Using Different Laser Parameters

Figure 5 shows that at low energy densities, the surface roughness of all laser-processed CoCrMo samples was comparable to that of the untreated substrate (30 nm). However, as the energy density increased, a higher input energy induced solid-to-liquid phase transitions in the alloy. Under the effects of the laser-generated pressure, molten material was ejected from the melt pool and redeposited along the laser irradiation direction [23], leading to surface irregularities and higher roughness. For the two nanosecond lasers, the roughness increased from around 30 nm to 480 nm as the energy density increased from 1273 to 1839 mJ/cm^2. Figure 6 shows that under low laser energy density conditions, nanosecond laser treatment did not significantly increase the surface hardness. However, femtosecond laser processing increased the hardness from 375 HV to 400 HV. As the energy density increased, all samples showed a corresponding improvement in hardness. Figure 7 shows the variation in the contact angle with the laser energy density for the samples treated first by laser irradiation and then by thermal annealing at 160 °C. At low energy densities, the contact angles of the two nanosecond-treated samples were similar to those of the untreated surface (90 ± 4°). However, the sample processed by the femtosecond laser exhibited a contact angle of more than 150°, indicating superhydrophobic behavior. As the energy density increased, the contact angles of both nanosecond systems increased, with the contact angle of the sample processed using a wavelength of 355 nm having a consistently higher value.

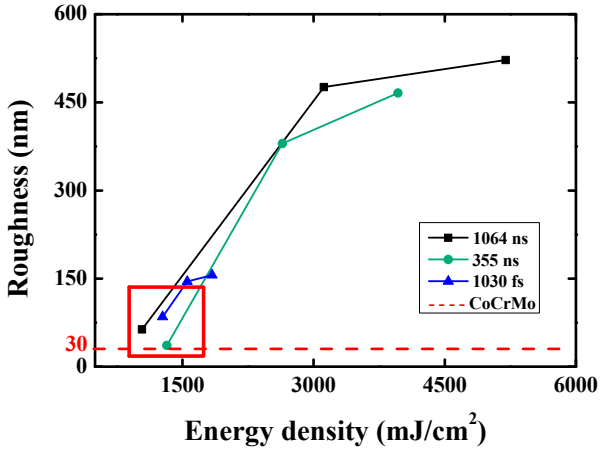

Figure 5. Surface roughness of CoCrMo samples after laser treatment.

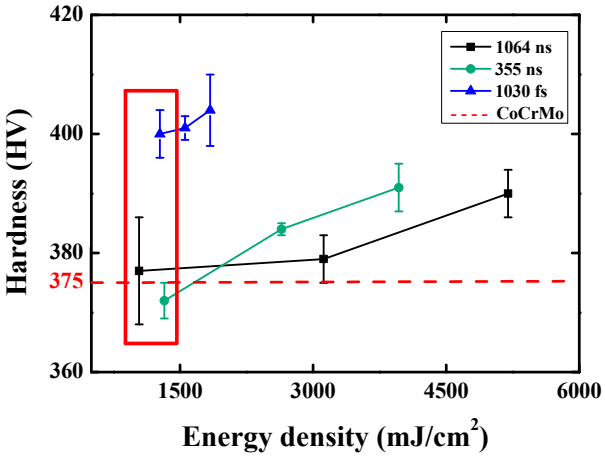

Figure 6. Surface hardness of CoCrMo samples after laser treatment.

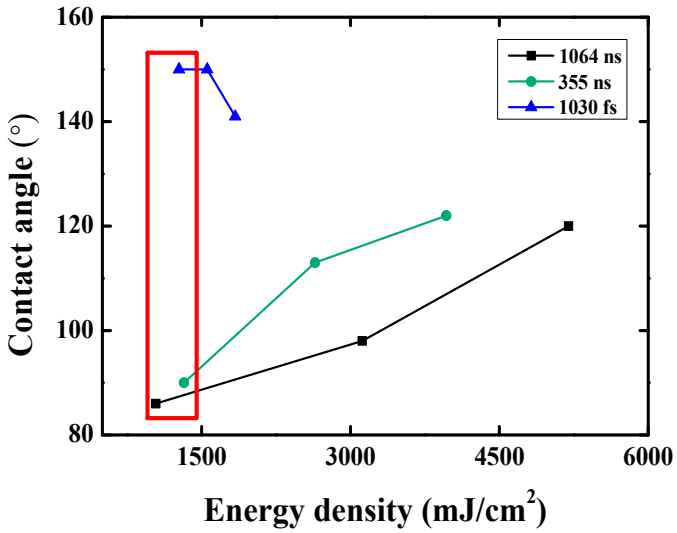

Figure 7. Contact angles of CoCrMo samples after combined laser and heat treatments.

3.3. Wear Resistance and Anti-Corrosion Behavior of CoCrMo Samples After Laser and Heat Treatment

Figure 8a shows the surface morphologies of the CoCrMo samples processed by femtosecond laser irradiation and heat treatment before and after the wear test. The wear process resulted in significant damage to the surface oxide layer (Figure 8b,c), with wear debris adhering to the surface (Figure 8d), resulting in an uneven surface topography and an inhomogeneous elemental distribution. Nonetheless, except for the sample processed by the nanosecond laser at an energy density of 1039 mJ/cm², the wear loss of all treated samples was lower than that of the untreated sample (1.4 mg). At low energy densities, the femtosecond-treated sample showed a lower wear loss (0.2 mg) than the samples treated by the nanosecond lasers with wavelengths of 1064 ns (1.5 mg) and 355 ns (1.3 mg), respectively. As the energy density increased, the wear loss in the nanosecond-treated samples decreased (Figure 9). In other words, a higher energy input is required to enhance wear resistance. In contrast, the femtosecond-treated sample exhibited a higher wear loss as the energy density increased from 1273 to 1839 mJ/cm². However, the wear loss was still significantly lower than that of the nanosecond samples. The correlation between the contact angle, hardness, and wear resistance suggests a multifactorial mechanism in which the surface chemistry, microstructure, and wettability collectively contribute to the tribological performance of CoCrMo samples. Figure 10 shows the Tafel plots of the CoCrMo samples following the laser and heat treatments. The corrosion current density of the 1030-fs sample was low. As shown in Figure 11, at similar energy densities, the corrosion current densities of the 1064-ns and 355-ns samples were comparable to that of the untreated material (112 nA/cm²). However, the corrosion current density of the 1030-fs sample was considerably lower (9 nA/cm²) owing to its hydrophobicity. As the energy density increased, the corrosion currents of the nanosecond samples decreased to 9 nA/cm² (1064-ns sample) and 26 nA/cm² (355-ns sample).

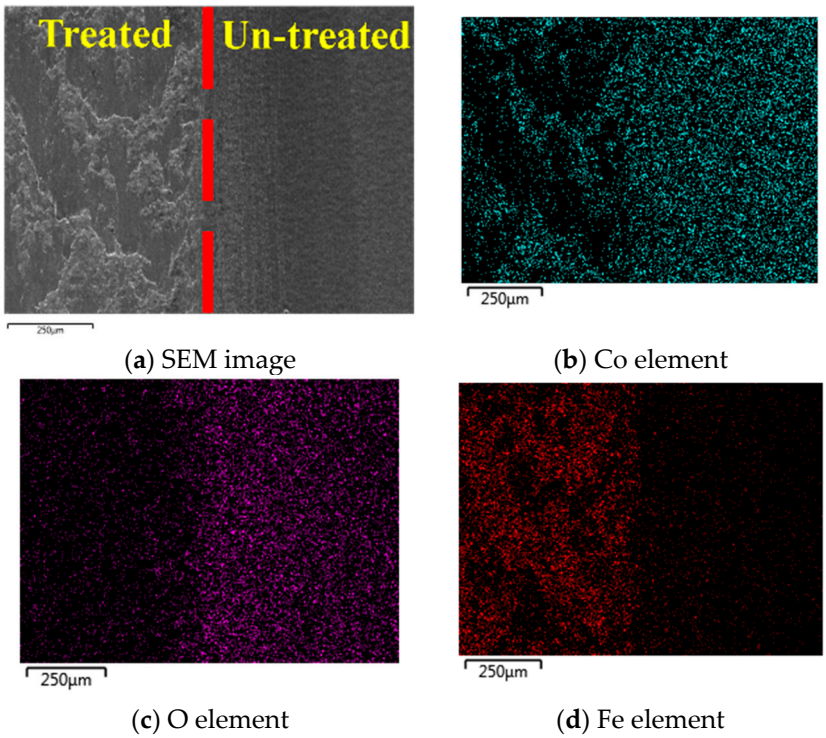

(**a**) SEM image (**b**) Co element

(**c**) O element (**d**) Fe element

Figure 8. Surface analysis of CoCrMo samples after wear test: (**a**) surface morphology and elemental composition; (**b**) Co element distribution; (**c**) O element distribution; and (**d**) Fe element distribution.

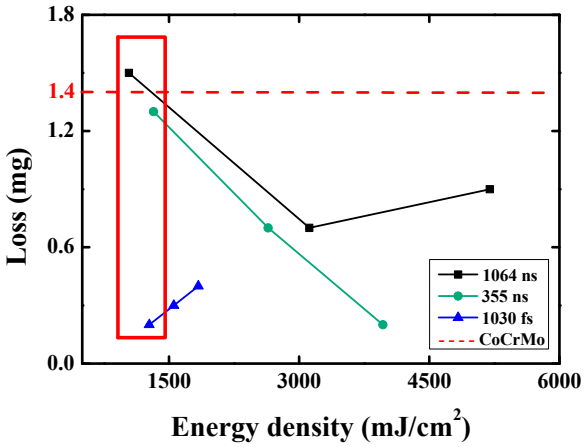

Figure 9. Wear loss of CoCrMo samples after combined laser and heat treatments.

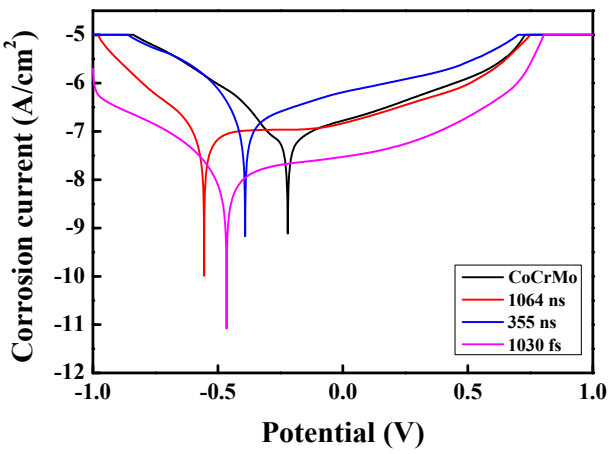

Figure 10. Tafel plots of CoCrMo samples after combined laser and heat treatments.

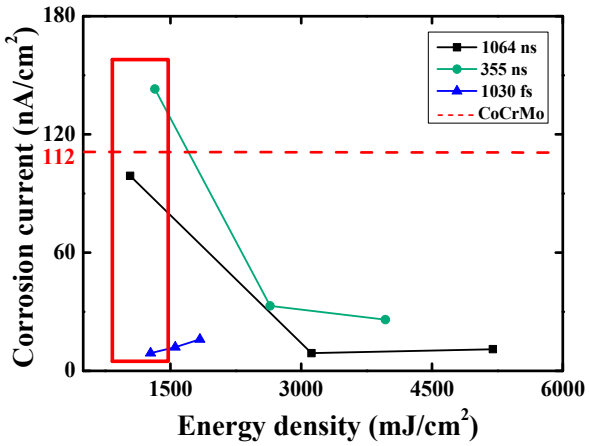

Figure 11. Corrosion current density of CoCrMo samples after combined laser and heat treatment.

4. Discussion

The femtosecond laser produced well-defined laser-induced periodic surface structures (LIPSS) on the treated surfaces. Although ultrashort-pulse lasers typically minimize thermal effects, oxidation can still occur in ambient air. Overall, the results suggest that while surface oxidation generally scales with increasing energy density, the relationship is not linear but depends on the type of laser and its processing parameters. In particular, femtosecond lasers induce greater oxidation at lower energies despite delivering a lower total energy input owing to their high peak power, localized energy deposition, and unique interaction mechanisms associated with ultrashort-pulse durations [24]. XRD patterns of the original CoCrMo sample and the three laser-processed samples. The original sample exhibited a dual-phase structure consisting of hexagonal close-packed (HCP) and face-centered cubic (FCC) phases. Following laser treatment, no significant changes in the crystal phases were observed. This finding, together with the elemental analysis results in Figure 3, indicates that the use of a femtosecond laser system can induce LIPSS structures without significantly altering either the surface phase composition or the elemental content. In other words, femtosecond laser structuring appears to be an effective surface modification technique for CoCrMo components that does not compromise their mechanical integrity. For the two nanosecond lasers, the roughness increased from around 30 nm to 480 nm as the energy density increased from 1273 to 1839 mJ/cm^2. For the femtosecond laser, an effective surface modification is achieved without compromising the mechanical dimensions. For biomedical implants, a higher surface roughness is beneficial for promoting early-stage osseointegration [25]. However, excessively rough surfaces may lead to debris entrapment and increased bacterial adhesion in vivo. Therefore, effective control of the surface topography through appropriate tuning of the laser parameters is essential to balance these competing outcomes. For the nanosecond laser samples, the hardness increased to approximately 391 HV and 390 HV at laser energies of 3965 and 5197 mJ/cm^2 for the 355 and 1064 nm laser systems, respectively. Similarly, for the femtosecond laser sample, the hardness increased to a maximum value of 404 HV at an energy intensity of 1839 mJ/cm^2. The present findings are consistent with those of Dunn [26], who reported that the use of a nanosecond laser to modify stainless steel surfaces induced the formation of an oxide layer at higher laser energy densities, which increased the surface hardness. A higher surface hardness reduces scratching, abrasion, and micro-motion-induced wear during joint articulation; therefore, it plays a key role in extending the functional lifespan of bio-implants in vivo [27].

In our previous study [20], a similar trend was observed. The transition to a steady-state hydrophobic condition occurred more slowly than that for the samples processed at

a lower laser power, but the final wettability of the surface increased. The initial hydrophilicity of the samples after laser treatment can be attributed to the formation of reactive oxides on their surfaces. In contrast, the contact angle of the femtosecond-treated sample decreased sharply as the energy density increased. Exir [28] reported that femtosecond laser processing, followed by aging, tends to increase the contact angles of alloys over time due to the gradual adsorption of organic matter on the surface and the entrapment of air in the periodic surface structures. Thus, in the present study, the reduction in the contact angle of the sample processed using the femtosecond laser system was most probably due to the loss of the LIPSS structures at higher energy densities, which led to the release of trapped air and a corresponding reduction in the surface hydrophobicity. The results in Figure 7 suggest that the surface wettability of CoCrMo implants can be tuned to suit specific clinical priorities, such as promoting cell attachment or minimizing bacterial adhesion, through appropriate control of the laser processing conditions. Li [29] found that laser treatment followed by annealing enhanced the corrosion resistance of H59 brass alloy by forming air pockets within the laser-induced structures. These air gaps acted as protective barriers, reducing contact between the corrosive medium and the alloy surface. Therefore, better corrosion resistance can be achieved owing to the superhydrophobic surface. Overall, the findings in Figure 11 show that femtosecond laser treatment provides excellent corrosion resistance, even without the formation of an oxide layer. This suggests that physical factors, such as surface geometry and wetting behavior, can be as influential as chemical passivation in determining the electrocorrosion properties of the CoCrMo alloy. In contrast, nanosecond laser treatment requires higher energy densities to achieve similar results, with the performance improvement being mainly the result of surface oxide formation. As shown in Figure 11, irrespective of the laser system employed, a higher contact angle led to a lower corrosion current density, indicating improved corrosion resistance. This finding is reasonable since a higher contact angle reduces the wetted surface area exposed to the electrolyte, thereby limiting electrochemical activity and ion exchange. Moreover, the results in Figures 8–11 demonstrate that, through appropriate control of the laser parameters and thermal annealing process (temperature and duration), the surface properties of CoCrMo implants can be precisely tuned to enhance wear resistance, corrosion protection, and wettability, thereby improving their performance in vivo.

Finally, the corrosion resistance properties of the CoCrMo samples subjected to combined laser processing and heat treatment were compared with those reported in the literature using two methods: (1) a direct comparison of the corrosion current and (2) a protection efficiency metric, defined as

$$\text{Protection}(\%) = \left(1 - \frac{I}{I_0}\right) \times 100\% \quad (4)$$

where I_0 is the corrosion current before treatment and I is the corrosion current after treatment.

A comparison of the corrosion performance of the current CoCrMo samples with the results presented in Table 2 [30–38] shows that some of the doped alloys in the literature, such as CoCrMoCu, exhibited a low corrosion current of 29.1 nA/cm^2. In the present study, the samples treated using the 1064-ns and 1030-fs laser systems and then annealed at 160 °C showed similar values (36 nA/cm^2). Since the initial current values varied across the different studies, the protection efficiency was considered to provide a more consistent basis for comparison. The protection efficiency was approximately 92% for the 1064-ns sample, 77% for the 355-ns sample, and 92% for the 1030-fs sample. These values are all close to those of the DLC coatings reported in the literature (up to 97.3%). In other words, laser processing combined with heat treatment provides an effective approach for

enhancing the corrosion resistance of CoCrMo implants, with optimized nanosecond laser systems achieving performance similar to that of femtosecond systems.

Table 2. Corrosion current and resistance properties of CoCrMo samples subjected to laser processing and heat treatment.

Sample	Thickness (nm)	I_{corr} (nA/cm²)	Protection (%)	Ref.
CoCrMo (CCM)	-	448	-	This work
CCM	-	328	-	[30]
CCM	-	40.5	-	[31]
CCM	-	39.8	-	[32]
CCM	-	39.5	-	[33]
CCM	-	30.9	-	[34]
CCM	-	18.0	-	[35]
TiN/CCM	2000	222	32.3	[30]
DLC/Ti/CCM	360/50	27.2	-	[36]
Ti-O/Ti/CCM	30/10	15.5	49.8	[34]
Ti-O/CCM	45	6.8	82.9	[32]
ZrN/CCM	1600	1.4	92.2	[35]
DLC/CCM	2200	1.08	97.3	[31]
CoCrWNi	-	444	-	[37]
CoCrMoW (5.3%)	-	194	-	[38]
CoCrMoCu (2%)	-	29.1	26.3	[33]
1064ns-low	-	396	11.61	This work
1064ns-medium	-	36	91.96	This work
1064ns-high	-	44	90.18	This work
355ns-low	-	572	-	This work
355ns-medium	-	132	70.54	This work
355ns-high	-	104	76.79	This work
1030fs-low	-	36	91.96	This work
1030fs-medium	-	48	89.29	This work
1030fs-high	-	64	85.71	This work

5. Conclusions

This study investigated the surface modification of a CoCrMo alloy using three laser systems (two nanosecond lasers and one femtosecond laser), followed by annealing at 160 °C for 2 h. The effects of laser wavelength and pulse duration on surface morphology, elemental composition, hardness, and surface roughness were comprehensively explored. The influence of laser treatment and annealing on the wettability, wear performance, and corrosion resistance of the various samples was also carefully examined. The experimental findings support the following main conclusions. As the laser energy density increased, an oxide layer was formed on the alloy surface, with the samples processed using the 355-ns system showing the highest oxygen content. The femtosecond laser generated laser-induced periodic microstructures (LIPSS) on the sample surface without altering its phase structure or surface composition. At similar low energy densities, the surface roughness of the samples processed by the nanosecond and femtosecond systems was comparable to that of an untreated substrate. However, the hardness produced by the femtosecond system (400 HV) was higher than that produced by the nanosecond system (377 HV). Femtosecond laser treatment followed by annealing produced a superhydrophobic surface. Wear loss decreased as the contact angle and surface hardness increased. The femtosecond system demonstrated the best wear resistance, with a wear loss of only 0.2 mg. The corrosion resistance decreased with increasing contact angle. The femtosecond system exhibited superior corrosion resistance (protection efficiency of approximately 92%), comparable to the values reported for other laser- and heat-treated samples in the literature.

In summary, the results presented in this study demonstrate that femtosecond laser processing, when combined with annealing at 160 °C, offers a promising route for enhancing the surface properties of CoCrMo biomedical implants. Compared to nanosecond laser systems, femtosecond-treated surfaces exhibit superior corrosion resistance, reduced wear, and unique microstructures, such as LIPSS, which contribute to superhydrophobic behavior. Given the critical role of surface properties in extending the service life of bioimplants, the present findings provide useful insights for the continued development of artificial metallic joints, particularly those targeted at patients with degenerative arthritis and other joint-related diseases.

Author Contributions: H.-K.L.: conceptualization, writing—original draft, writing—review & editing, and funding acquisition. P.-W.C.: methodology, investigation, data curation, and writing—original draft. Y.-M.D.: investigation, formal analysis. Y.-T.L.: formal analysis and writing—review & editing. Y.-J.C.: investigation, formal analysis. W.-H.L.: conceptualization, writing—review & editing. All authors have discussed the results and commented on the manuscript. All authors have read and agreed to the published version of the manuscript.

Funding: This research was funded by the National Science and Technology Council, ROC, under Project No. NSTC 114-2221-E-020-016.

Data Availability Statement: The raw data supporting the conclusions of this article will be made available by the authors on request.

Conflicts of Interest: The authors declare no conflicts of interest.

References

1. Li, Z. Advancements of biomaterial in hip replacement technology incorporating ceramic materials. *J. Orthop.* **2025**, *62*, 27–35.
2. Long, M.; Rack, H. Titanium alloys in total joint replacement—A materials science perspective. *Biomaterials* **1998**, *19*, 1621–1639.
3. Niinomi, M. Mechanical properties of biomedical titanium alloys. *Mater. Sci. Eng. A* **1998**, *243*, 231–236.
4. Hermawan, H.; Ramdan, D.; Djuansjah, J.R. Metals for biomedical applications. *Biomed. Eng.-Theory Appl.* **2011**, *1*, 411–430.
5. Niinomi, M. Recent metallic materials for biomedical applications. *Metall. Mater. Trans. A* **2002**, *33*, 477–486.
6. Buford, A.; Goswami, T. Review of wear mechanisms in hip implants: Paper I—General. *Mater. Des.* **2004**, *25*, 385–393.
7. Saldívar-García, A.; López, H. Microstructural effects on the wear resistance of wrought and as-cast Co-Cr-Mo-C implant alloys. *J. Biomed. Mater. Res. Part A* **2005**, *74*, 269–274.
8. Liao, Y.; Pourzal, R.; Stemmer, P.; Wimmer, M.; Jacobs, J.; Fischer, A.; Marks, L. New insights into hard phases of CoCrMo metal-on-metal hip replacements. *J. Mech. Behav. Biomed. Mater.* **2012**, *12*, 39–49.
9. Lashgari, H.; Zangeneh, S.; Hasanabadi, F.; Saghafi, M. Microstructural evolution during isothermal aging and strain-induced transformation followed by isothermal aging in Co-Cr-Mo-C alloy: A comparative study. *Mater. Sci. Eng. A* **2010**, *527*, 4082–4091.
10. Toh, S.M.S.; Ashkanfar, A.; English, R.; Rothwell, G. Computational method for bearing surface wear prediction in total hip replacements. *J. Mech. Behav. Biomed. Mater.* **2021**, *119*, 104507.
11. Qiang, L.; Zhang, B.; Zhou, Y.; Zhang, J. Improving the internal stress and wear resistance of DLC film by low content Ti doping. *Solid State Sci.* **2013**, *20*, 17–22.
12. Kusmanov, S.; Silkin, S.; Smirnov, A.; Belkin, P. Possibilities of increasing wear resistance of steel surface by plasma electrolytic treatment. *Wear* **2017**, *386*, 239–246.
13. Wagner, J.; Mitterer, C.; Penoy, M.; Michotte, C.; Wallgram, W.; Kathrein, M. The effect of deposition temperature on microstructure and properties of thermal CVD TiN coatings. *Int. J. Refract. Met. Hard Mater.* **2008**, *26*, 120–126.
14. Liao, L.; Gao, R.; Yang, Z.; Wu, S.; Wan, Q. A study on the wear and corrosion resistance of high-entropy alloy treated with laser shock peening and PVD coating. *Surf. Coat. Technol.* **2022**, *437*, 128281.
15. Pan, X.; Zhou, L.; Hu, D.; He, W.; Liu, P.; Yu, Z.; Liang, X. Superior wear resistance in cast aluminum alloy via femtosecond laser induced periodic surface structures and surface hardening layer. *Appl. Surf. Sci.* **2023**, *636*, 157866.
16. Yu, Y.; Zhou, L.; Cai, Z.; Luo, S.; Pan, X.; Zhou, J.; He, W. Research on the mechanism of DD6 single crystal superalloy wear resistance improvement by femtosecond laser modification. *Appl. Surf. Sci.* **2022**, *577*, 151691.

17. Ngo, C.-V.; Chun, D.-M. Fast wettability transition from hydrophilic to superhydrophobic laser-textured stainless steel surfaces under low-temperature annealing. *Appl. Surf. Sci.* **2017**, *409*, 232–240.
18. Chichkov, B.N.; Momma, C.; Nolte, S.; Von Alvensleben, F.; Tünnermann, A. Femtosecond, picosecond and nanosecond laser ablation of solids. *Appl. Phys. A* **1996**, *63*, 109–115.
19. Yang, L.; Ding, X.; Zhou, Y. Femtosecond laser induced periodic nanostructures towards enhanced anti-corrosive property of titanium. *Surf. Coat. Technol.* **2023**, *463*, 129533.
20. Lin, H.-K.; Yang, S.-J.; Chang, P.-W.; Lu, W.-H.; Chang, Y.-J. Effects of laser patterning and heat treatment on hydrophobicity, wear, and corrosion resistance of 316L stainless steel. *Int. J. Adv. Manuf. Technol.* **2025**, *137*, 5511–5520.
21. Vaghasiya, H.; Miclea, P.-T. Investigating Laser-Induced Periodic Surface Structures (LIPSS) Formation in Silicon and Their Impact on Surface-Enhanced Raman Spectroscopy (SERS). *Optics* **2023**, *4*, 538–550.
22. Fava, A.; Kaciulis, S.; Mezzi, A.; Montanari, R.; Palombi, A.; Varone, A. XPS Study of Co28Cr6Mo Biocompatible Alloy. *Surf. Interface Anal.* **2025**. https://doi.org/10.1002/sia.70009.
23. Cui, M.; Huang, C.; Jiang, Q.; Xiao, R.; Huang, T. Understanding the effect of oxide accumulation on femtosecond laser machining of nickel-based superalloy alloy. *Appl. Surf. Sci.* **2025**, *705*, 163543.
24. Earl, C.; Castrejón-Pita, J.; Hilton, P.; O'Neill, W. The dynamics of laser surface modification. *J. Manuf. Process.* **2016**, *21*, 214–223.
25. Hong, T.F. Laser Surface Modification for Rapid Oxide Layer Formation on Ti-6Al-4V. *J. Laser Micro/Nanoeng.* **2014**, *9*, 64–67.
26. Dunn, A.; Carstensen, J.V.; Wlodarczyk, K.L.; Hansen, E.B.; Gabzdyl, J.; Harrison, P.M.; Shephard, J.D.; Hand, D.P. Nanosecond laser texturing for high friction applications. *Opt. Lasers Eng.* **2014**, *62*, 9–16.
27. Moghadasi, K.; Isa, M.S.M.; Ariffin, M.A.; Mohd jamil, M.Z.; Raja, S.; Wu, B.; Yamani, M.; Muhamad, M.R.B.; Yusof, F.; Jamaludin, M.F.; et al. A review on biomedical implant materials and the effect of friction stir based techniques on their mechanical and tribological properties. *J. Mater. Res. Technol.* **2022**, *17*, 1054–1121.
28. Exir, H.; Weck, A. Mechanism of superhydrophilic to superhydrophobic transition of femtosecond laser-induced periodic surface structures on titanium. *Surf. Coat. Technol.* **2019**, *378*, 124931.
29. Li, X.; Jiang, Y.; Jiang, Z.; Li, Y.; Wen, C.; Zhang, D.; Lian, J.; Zhang, Z. Improvement of corrosion resistance of H59 brass through fabricating superhydrophobic surface using laser ablation and heating treatment. *Corros. Sci.* **2021**, *180*, 109186.
30. Jakovljević, S.; Alar, V.; Ivanković, A. Electrochemical behaviour of PACVD TiN-coated CoCrMo medical alloy. *Metals* **2017**, *7*, 231.
31. Zhang, T.; Deng, Q.; Liu, B.; Wu, B.; Jing, F.; Leng, Y.; Huang, N. Wear and corrosion properties of diamond like carbon (DLC) coating on stainless steel, CoCrMo and Ti6Al4V substrates. *Surf. Coat. Technol.* **2015**, *273*, 12–19.
32. Xie, D.; Wang, H.; Ganesan, R.; Leng, Y.; Sun, H.; Huang, N. Fatigue durability and corrosion resistance of TiO_2 films on CoCrMo alloy under cyclic deformation. *Surf. Coat. Technol.* **2015**, *275*, 252–259.
33. Gan, Y.; Zhou, M.; Ji, C.; Huang, G.; Chen, Y.; Li, L.; Huang, T.; Lu, Y.; Lin, J. Tailoring the tribology property and corrosion resistance of selective laser melted CoCrMo alloys by varying copper content. *Mater. Des.* **2023**, *228*, 111869.
34. Chen, S.; Wu, B.; Xie, D.; Jiang, F.; Liu, J.; Sun, H.; Zhu, S.; Bai, B.; Leng, Y.; Huang, N. The adhesion and corrosion resistance of Ti–O films on CoCrMo alloy fabricated by high power pulsed magnetron sputtering (HPPMS). *Surf. Coat. Technol.* **2014**, *252*, 8–14.
35. Corona-Gomez, J.; Sandhi, K.; Yang, Q. Wear and corrosion behaviour of nanocrystalline TaN, ZrN, and TaZrN coatings deposited on biomedical grade CoCrMo alloy. *J. Mech. Behav. Biomed. Mater.* **2022**, *130*, 105228.
36. Zhang, T.; Liu, B.; Wu, B.; Liu, J.; Sun, H.; Leng, Y.; Huang, N. The stability of DLC film on nitrided CoCrMo alloy in phosphate buffer solution. *Appl. Surf. Sci.* **2014**, *308*, 100–105.
37. Wang, R.; Wang, R.; Chen, D.; Qin, G.; Zhang, E. Novel CoCrWNi alloys with Cu addition: Microstructure, mechanical properties, corrosion properties and biocompatibility. *J. Alloys Compd.* **2020**, *824*, 153924.
38. Hu, Y.; Dong, C.; Kong, D.; Ding, J.; He, X.; Ni, X.; Zhang, L.; Li, X. Effects of post-production heat treatment on the mechanical and corrosion behaviour of CoCrMoW alloy manufactured through selective laser melting. *Mater. Today Commun.* **2021**, *29*, 102994.